Probing the Structure and Bonding in Al_6N^- and Al_6N by Photoelectron Spectroscopy and Ab Initio Calculations

Boris B. Averkiev and Alexander I. Boldyrev*

0300 Old Main Hill, Utah State University, Department of Chemistry and Biochemistry, Logan, Utah 84322-0300

Xi Li† and Lai-Sheng Wang*

Department of Physics, Washington State University, 2710 University Drive, Richland, Washington 99354, and Chemical Sciences Division, Pacific Northwest National Laboratory, MS K8-88, P.O. Box 999, Richland, Washington 99352

Received: October 13, 2006; In Final Form: November 2, 2006

The electronic and geometrical structure of a nitrogen-doped Al_6^- cluster (Al_6N^-) is investigated using photoelectron spectroscopy and ab initio calculations. Photoelectron spectra of Al_6N^- have been obtained at three photon energies with seven resolved spectral features. The electron affinity of Al_6N has been determined to be 2.58 ± 0.04 eV. Global minimum structure searches for A_6N^- and its corresponding neutral form are performed using several theoretical methods. Vertical electron detachment energies, calculated using three different methods for the lowest energy structure and a low-lying isomer, are compared with the experimental data. The ground-state structure of Al_6N^- is established from the joint experimental and theoretical study to consist of an Al_2 dimer bonded to the top of a quasi-planar tetracoordinated N unit, Al_4N^-, or it can be viewed as a distorted trigonal prism structure with the N atom bonded in one of the prism faces. For neutral Al_6N, three low-lying isomers are found to compete for the global minimum, two of which are built from the tetracoordinated Al_4N unit. The chemical bonding in Al_6N^- is discussed on the basis of molecular orbital and natural bond analyses.

1. Introduction

Aluminum nitride is an important semiconductor material, but there have been relatively few experimental and theoretical studies on small aluminum nitride clusters.[1−11] Recently, Li and Wang reported an extensive set of photoelectron spectra of Al_xN^- clusters where $x = 2-22$ at 193 nm and compared them to those of pure Al_x^- clusters.[10] They found spectral similarity between Al_xN^- and Al_{x-1}^- and suggested that there is a strong charge transfer to form formally N^{3-} in the nitrogen-doped aluminum clusters. In a very recent study,[12] we combined photoelectron spectroscopy (PES) with global minimum structural search, using a gradient-embedded genetic algorithm followed by high-level ab initio calculations, to elucidate the structures and bonding for a series of nitrogen-doped small aluminum clusters, Al_xN^- ($x = 3-5$). Vertical electron detachment energies calculated for the lowest-energy structures were found to be in excellent agreement with the experimental observations. Planar structures were established for all the three Al_xN^- ($x = 3-5$) anions. In particular, we found that Al_4N^- is a highly stable cluster, isoelectronic to the penta-atomic tetracoordianted planar carbon molecule, CAl_4^{2-}.[13,14] The global minimum structure of Al_5N^- simply consists of a planar Al_4N^- with the extra Al atom bonded to its side in the same plane,[12] suggesting the stability and robustness of the planar tetracoordinated N structural unit. In the current article, we report a joint PES and ab inito study on Al_6N^- and Al_6N to examine if the planar Al_4N structural unit plays any role in larger N-doped aluminum clusters.

For the Al_6N cluster, a number of different structures have been suggested from prior theoretical studies,[3,7−9] but there is no consensus about its global minimum. Nayak, Khanna, and Jena[3] reported a global minimum structure with the N atom capping the triangular face of a distorted Al_6 octahedron. Leskiw et al.[7] and Guo and Wu[9] reported a global minimum structure with the N atom located inside a distorted Al_6 octahedron. Ling, Song, and Cao[8] reported a very low symmetry structure, which can be approximately viewed as a N atom inside a highly distorted Al_6 prism structure.

In the current work, well-resolved photoelectron spectra of Al_6N^- at three photon energies are compared to theoretical calculations. We found that Al_6N^- possesses a C_{2v} global minimum structure, which consists of an Al_2 dimer bonded on the top of a planar Al_4N^- unit. It can also be viewed as an N atom located in one of the faces of a distorted Al_6 trigonal prism. For neutral Al_6N, we found three low-lying isomers with very close energies competing for the global minimum. Two of the three low-lying structures are related to the planar Al_4N, confirming the stability and robustness of the planar tetracoordinated N structural unit.

2. Experimental Method

The experiment was performed using a magnetic-bottle PES apparatus with a laser vaporization cluster source, details of which have been published elsewhere.[15] Briefly, the Al_6N^-

* Corresponding authors. E-mail: boldyrev@cc.usu.edu (Boldyrev); ls.wang@pnl.gov (Wang).

† Current address: Rowland Institute at Harvard, Harvard University, 100 Edwin H. Land Blvd., Cambridge, MA 02142.

10.1021/jp066747e CCC: $37.00
Published on Web 12/14/2006

clusters were produced by laser vaporization of a pure Al disk target with a 5% N_2/He carrier gas. Under this condition, only clusters doped with one nitrogen atom were formed.[10] The Al_6N^- anion clusters of interest were size-selected and decelerated before crossing with a detachment laser beam. We have reported PES spectra of Al_xN^- for $x = 2-22$ at 193 nm (6.424 eV) recently along with the Al_xN^- mass distribution.[10] In the current study, we have obtained additional photoelectron spectra for Al_6N^- at two lower photon energies, 355 (3.496 eV) and 266 (4.661 eV). The lower photon energy spectra yielded better-resolved spectra, which were necessary to compare with theoretical calculations. The electron energy resolution of our PES apparatus was $\Delta E/E \sim 3\%$, that is, about 30 meV for 1-eV electrons.

3. Theoretical Methods

We performed an initial search for the global minimum of Al_6N^- and Al_6N using our gradient embedded genetic algorithm (GEGA) program.[16,17] We used a hybrid method known in the literature as B3LYP[18−20] with the small split-valence basis sets (3-21G)[21] for energy, gradient, and force calculations. We reoptimized geometries and calculated frequencies for all isomers found for Al_6N^- and Al_6N at the B3LYP/6-311+G* level of theory. We also recalculated the two lowest-energy structures of Al_6N^- using a coupled-cluster method with single, double, and noniterative triple excitations (CCSD(T))[22−24] on the basis of the RHF formalism with the polarized split-valence basis sets (6-311+G*).[25−27] Total energies of the local minimum structures were also recalculated at the CCSD(T)/6-311+G-(2df)//B3LYP/6-311+G* level of theory. We performed additional single-point calculations at the multi-configuration self-consistent field method (CASSCF(X,Y)[28,29] with *X* active electrons and *Y* active molecular orbitals in order to test the validity of the one-electron approximation.

The Al_6N^- vertical electron detachment energies (VDEs) were calculated using the R(U)CCSD(T)/6-311+G(2df), the outer valence Green Function method (ROVGF/6-311+G(2df))[30−34] at the RCCSD(T)/6-311+G* geometries, and the time-dependent DFT method[35,36] (TD-B3LYP/6-311+G(2df)) at the B3LYP/6-311+G* geometries. Core electrons were frozen in treating the electron correlation at the RCCSD(T) and ROVGF levels of theory.

The B3LYP, R(U)CCSD(T), and R(U)OVGF ab initio calculations were performed using the Gaussian 98 and 03 programs.[37,38] Molecular orbital visualization has been done using the MOLDEN3.4 program.[39]

4. Experimental Results

The PES spectra of Al_6N^- at three photon energies are shown in Figure 1. Two bands were observed in the 355-nm spectrum (Figure 1a), a relatively sharp band (X) at a VDE of 2.66 eV and a broadband, which seemed to consist of two overlapping features (A and B). A long tail was observed at the lower binding energy side, which depended on the detachment photon flux at 355 nm and was due to thermionic emission processes.[40] The thermionic emission was less severe at higher photon energies because of the relatively lower photon fluxes used. The X band was relatively sharp, suggesting a small geometrical change from the ground state of Al_6N^- to that of neutral Al_6N. From the onset of the X band, we obtained an adiabatic detachment energy (ADE) of 2.58 ± 0.04 eV, which defines the electron affinity of neutral Al_6N. At 266 nm (Figure 1b), the bands A and B were resolved more clearly and a number of new features were also revealed. Two relatively sharp peaks were observed at 4.00

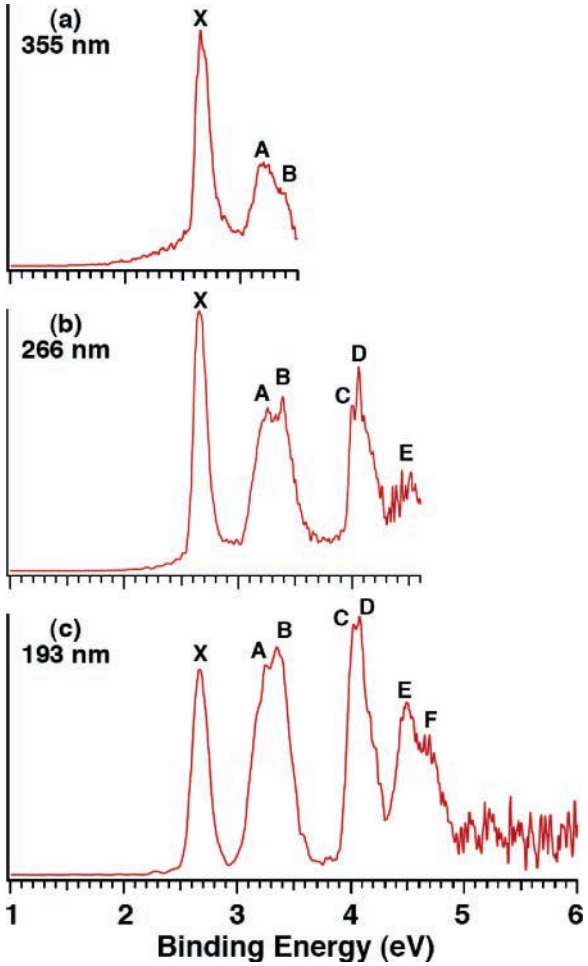

Figure 1. Photoelectron spectra of Al_6N^- at (a) 355 nm (3.496 eV), (b) 266 nm (4.661 eV), and (c) 193 nm (6.424 eV).

eV (C) and 4.06 eV (D), which could be due to the 0−0 and 0−1 transitions of a vibrational progression. However, since there were no other regular peaks with a similar spacing at higher binding energies beyond peak D, we tentatively assigned the C and D as the origins of two electronic transitions. As will be shown below, these assignments were born out in our theoretical calculations. At 193 nm (Figure 1c), two more closely spaced bands were observed at VDEs of 4.51 eV (E) and 4.70 eV (F). In addition, the relative intensities of the A and B bands, as well as the C and D bands, appeared to increase with the photon energies.

The VDEs of all the observed bands are given in Tables 1 and 2, where they are compared with theoretical calculations for the two lowest-lying isomers of Al_6N^-.

5. Theoretical Results

Al_6N^-. We initially performed the GEGA search for the global minimum structure at B3LYP/3-21G level of theory separately for both singlet and triplet states. Figure 2 displays the low-lying structures found by the GEGA search and recalculated at the B3LYP/6-311+G* geometry with relative total energies at CCSD(T)/6-311+G(2df)//B3LYP/6-311+G*.

The structure II (Figure 2) was found by GEGA at the B3LYP/3-21G level to be the global minimum, which is the same as reported by Leskiw et al.[7] and Guo and Wu.[9] However, at the B3LYP/6-311+G*, CCSD(T)/6-311+G*, and CCSD(T)/6-311+G(2df)//B3LYP/6-311+G* levels of theory, the global minimum is the structure I, which is more stable than the

TABLE 1: Comparison of the Experimental VDEs to the Calculated VDEs for the Structure I of Al_6N^- (All Energies in eV)

feature	VDE (expt)[a]	final state and electronic configuration	VDE (theor.) TD-B3LYP	VDE (theor.) OVGF[b]	VDE (theor.) ΔCCSD(T)
X	2.66 (3)	$^2B_1$, $2b_2^2 4a_1^2 2\ b_1^2 1a_2^2 3b_2^2 5a_1^2 3b_1^1$	2.41	2.53 (0.86)	2.63
A	3.25 (5)	$^2A_1$, $2b_2^2 4a_1^2 2\ b_1^2 1a_2^2 3b_2^2 5a_1^1 3b_1^2$	3.14	3.30 (0.86)	3.36
B	3.40 (4)	$^2B_2$, $2b_2^2 4a_1^2 2\ b_1^2 1a_2^2 3b_2^1 5a_1^2 3b_1^2$	3.22	3.44 (0.86)	3.44
C	4.00 (3)	$^2A_2$, $2b_2^2 4a_1^2 2\ b_1^2 1a_2^1 3b_2^2 5a_1^2 3b_1^2$	4.21	4.20 (0.83)	4.23
D	4.06 (3)	$^2B_1$, $2b_2^2 4a_1^2 2\ b_1^1 1a_2^2 3b_2^2 5a_1^2 3b_1^2$	4.00	4.21 (0.82)	*c*
E	4.50 (5)	$^2A_1$, $2b_2^2 4a_1^1 2\ b_1^2 1a_2^2 3b_2^2 5a_1^2 3b_1^2$	4.40	4.51 (0.81)	*c*
F	4.70 (5)	$^2B_2$, $2b_2^1 4a_1^2 2\ b_1^2 1a_2^2 3b_2^2 5a_1^2 3b_1^2$	4.62	4.70 (0.81)	*c*

[a] Numbers in parentheses represent the uncertainty in the last digit. [b] Values in parentheses represent the pole strength of the OVGF calculation. [c] This value cannot be calculated at the this level of theory.

TABLE 2: Comparison of Experimental VDEs to the Calculated VDEs for the Structure II of Al_6N^- (All Energies in eV)

feature	VDE (expt)[a]	final state and electronic configuration	VDE (theor.) TD-B3LYP	VDE (theor.) OVGF[b]	VDE (theor.) ΔCCSD(T)
X	2.66 (3)	$^2A_1$, $2b_2^2 2b_1^2 4a_1\ ^2 3b_2^2 5a_1^2 1a_2^2 6a_1^1$	2.56	2.67 (0.86)	2.79
A	3.25 (5)	$^2A_2$, $2b_2^2 2b_1^2 4a_1\ ^2 3b_2^2 5a_1^2 1a_2^1 6a_1^2$	2.78	2.95 (0.86)	2.99
B	3.40 (4)	$^2A_1$, $2b_2^2 2b_1^2 4a_1\ ^2 3b_2^2 5a_1^1 1a_2^2 6a_1^2$	3.64	3.73 (0.86)	*c*
C	4.00 (3)	$^2B_2$, $2b_2^2 2b_1^2 4a_1\ ^2 3b_2^1 5a_1^2 1a_2^2 6a_1^2$	3.87	4.10 (0.84)	3.98
D	4.06 (3)	$^2A_1$, $2b_2^2 2b_1^2 4a_1\ ^1 3b_2^1 5a_1^2 1a_2^2 6a_1^2$	4.11	4.31 (0.82)	*c*
E	4.50 (5)	$^2B_1$, $2b_2^2 2b_1^1 4a_1\ ^2 3b_2^2 5a_1^2 1a_2^2 6a_1^2$	4.06	4.29 (0.80)	4.23
F	4.70 (5)	$^2B_2$, $2b_2^1 2b_1^2 4a_1\ ^2 3b_2^2 5a_1^2 1a_2^2 6a_1^2$	4.81	4.89 (0.79)	*c*

[a] Numbers in parentheses represent the uncertainty in the last digit. [b] Values in parentheses represent the pole strength of the OVGF calculation. [c] This value cannot be calculated at this level of theory.

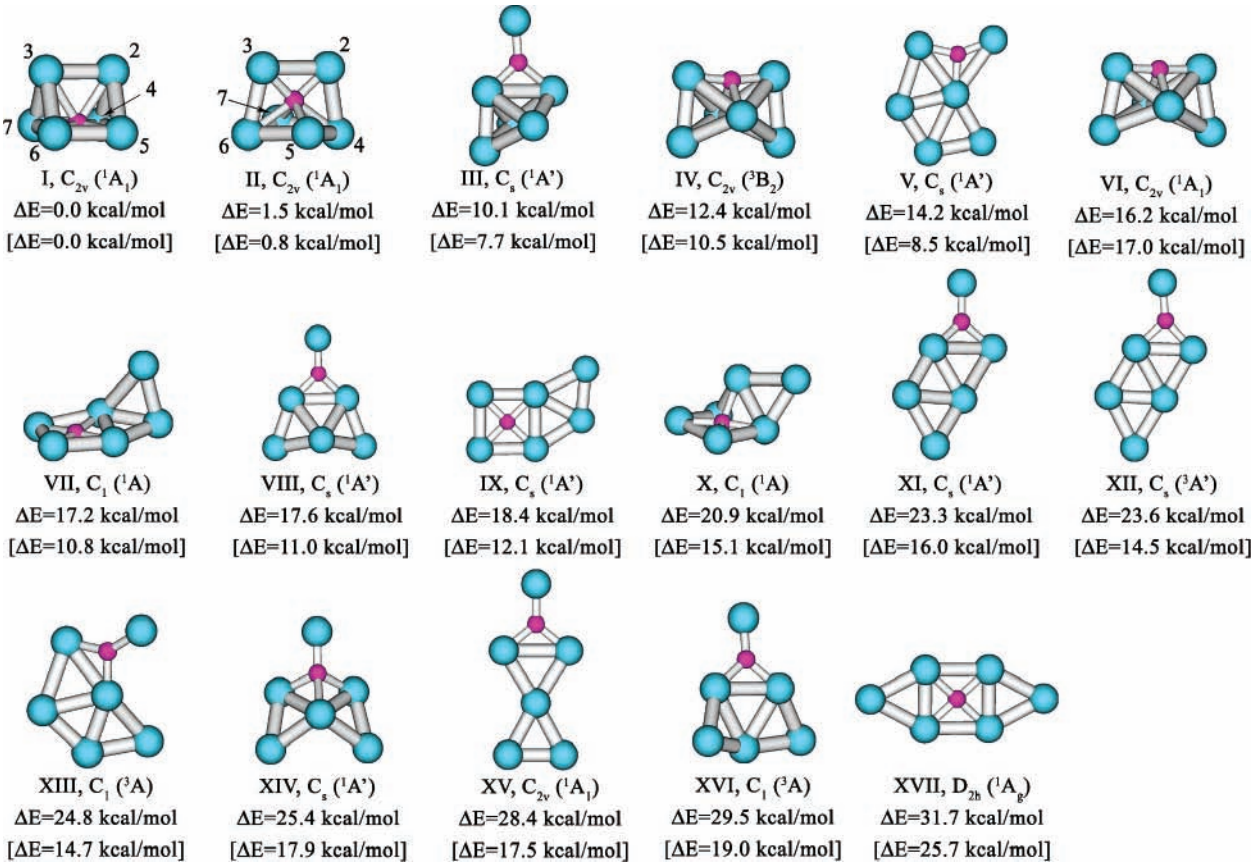

Figure 2. Computationally found isomers for Al6N$^-$. Relative energies are given at CCSD(T)/6-311+G(2df)//B3LYP/6-311+G* and at B3LYP/6-311+G* in parentheses.

structure II at the above levels of theory by 0.8, 2.4, and 1.5 kcal/mol, respectively. The Hatree-Fock function was found to be dominant ($C_{HF} = 0.951$ out of 31 878 configurations) in CASSCF(10,10)/6-311+G* calculations for the structure I. The global minimum structure I seems to have been missed in previous studies of Al_6N^-. At CCSD(T)/6-311+G*, the structure II has one imaginary frequency (Table 3). However, the vibrationally averaged structure II can be considered to have the C_{2v} symmetry. Among other low-lying isomers, we mention the structure III, which consists of an NAl moiety bonded to a capped-tetrahedral Al_5 cluster, is higher in energy than the global minimum structure by 7.7 kcal/mol (B3LYP/6-311+G*) and 10.1 (CCSD(T)/6-311+G(2df)//B3LYP/6-311+G*). The lowest triplet structure IV, which is related to the singlet structure II,

TABLE 3: Molecular Properties of the Al_6N^- Species

molecular parameter	(C_{2v}, $^1A_1$)		II (C_{2v}, $^1A_1$)		II (C_s, $^1A'$)
	B3LYP/ 6-311+G*	CCSD(T)/6-311+G*	B3LYP/6-311+G*	CCSD(T)/6-311+G*	CCSD(T)/6-311+G*
E, a.u.	−1509.59658 59	−1506.68285 19	−1509.59523 94	−1506.67910 67	−1506.67963 13
R(N−Al_2)	2.391	2.355	1.931	1.930	1.945
R(N−Al_4)	2.004	2.004	2.333	2.340	2.296
R(N−Al_5)			2.094	2.078	2.019
R(N−Al_7)					2.193
R(Al_2−Al_3)	2.614	2.616	2.795	2.826	2.771
R(Al_2−Al_4)	2.672	2.683	2.726	2.723	2.698
R(Al_4−Al_5)	3.010	2.975	2.634	2.637	2.648
R(Al_4−Al_7)					2.607
R(Al_5−Al_6)	2.615	2.628			
ω_1, cm^{-1}	a_1, 367 (17)	385	a_1, 561 (198)	573	
ω_2, cm^{-1}	a_1, 323 (82)	349	a_1, 339 (4)	350	
ω_3, cm^{-1}	a_1, 291 (2)	297	a_1, 253 (3)	259	
ω_4, cm^{-1}	a_1, 259 (17)	271	a_1, 216 (7)	225	
ω_5, cm^{-1}	a_1, 204 (5)	212	a_1, 117 (11)	120	
ω_6, cm^{-1}	a_2, 245 (0)	252	a_1, 115 (0)	104	
ω_7, cm^{-1}	a_2, 185 (0)	181	a_2, 286 (0)	287	
ω_8, cm^{-1}	a_2, 63 (0)	48	a_2, 64 (0)	52i	
ω_9, cm^{-1}	b_1, 536 (77)	536	b_1, 332 (12)	360	
ω_{10}, cm^{-1}	b_1, 272 (10)	276	b_1, 229 (18)	232	
ω_{11}, cm^{-1}	b_1, 188 (8)	183	b_1, 30 (0)	113i	
ω_{12}, cm^{-1}	b_2, 526 (131)	542	b_2, 550 (150)	564	
ω_{13}, cm^{-1}	b_2, 250 (13)	242	b_2, 278 (2)	282	
ω_{14}, cm^{-1}	b_2, 109 (12)	101	b_2, 194 (0)	193	
ω_{15}, cm^{-1}	b_2, 80 (1)	56	b_2 108 (30)	84	

[a] Values in parentheses represent relative absorbance intensities in the IR spectrum (km/ mol).

is higher in energy than the global minimum structure by 10.5 kcal/mol (B3LYP/6-311+G*) and 12.4 (CCSD(T)/ 6-311+G-(2df)//B3LYP/6-311+G*). We also identified a number of local minimum structures (Figure 2) with energies between 14 and 32 kcal/mol above the global minimum.

Al_6N. We initially performed the GEGA search for the global minimum structure of neutral Al_6N at the B3LYP/3-21G level of theory separately for doublet and quartet states. Figure 3 shows the low-lying structures found by the GEGA search and recalculated at the B3LYP/6-311+G* geometry with relative total energies at CCSD(T)/6-311+G(2df)//B3LYP/6-311+G*.

The global minimum structure XVIII (Figure 3) at the B3LYP/3-21G level found by GEGA is the same as that reported by Leskiw et al.[7] and Guo and Wu.[9] Ling, Song, and Cao[8] found a global minimum structure similar to the structure XVIII, but without any symmetry. Note the structure XVIII in Figure 3 possesses C_{2v} symmetry. Nayak, Khanna, and Jena[3] reported a global minimum structure for Al_6N, in which a nitrogen atom is coordinated outside the face of a distorted Al_6 octahedron. However, at the B3LYP/6-311+G* level of theory the global minimum is the structure XIX, which has never been reported in the literature. At our highest CCSD(T)/6-311+G(2df)// B3LYP/6-311+G* level of theory the structure XVIII again becomes the most stable one, but it is only more stable than structure XIX by 0.7 kcal/mol. We also found that the structure XX, which corresponds to the global minimum of the anion (structure I), is also a very stable structure for the neutral species, only 3.3 kcal/mol (B3LYP/6-311+G*) and 0.8 kcal/mol (CCSD-(T)/6-311+G(2df)// B3LYP/6-311+G*) higher than the structure XVIII. In order to avoid the problem with a different spin-contamination at the UCCSD(T)/6-311+G(2df) level of theory for structures XVIII−XX, we evaluated energies of the structures XVIII−XX as a difference between total energy of the anion at the geometry of the neutral species (at RCCSD(T)/6-311+G(2df)//B3LYP/6-311+G*) and the first vertical electron detachment energy for the anion (at ROVGF/6-311+G(2df)// B3LYP/6-311+G*) at the geometry of the neutral species. In that approach the $\langle S^2 \rangle$ values are exactly 0.750. The structure XVIII was found again to be the global minimum with relative energies equal to 3.7 kcal/mol for the structure XIX and 1.8 kcal/mol for the structure XX. The energy differences for the three low-lying structures of Al_6N (XVIII, XIX, XX) are too small to allow us to conclude with certainty which one is the true global minimum. Notably, all other isomers, XXI−XXXIII in Figure 3, are significantly higher in energy and will not be discussed further.

The molecular properties for the two low-lying structures of Al_6N^- (I and II) and the three low-lying structures of Al_6N (XVIII, XIX, and XX) are summarized in Tables 3 and 4, respectively.

6. Interpretations of the PES Spectra and Comparison with the Calculated VDEs

We calculated the VDEs for structures I and II of Al_6N^- at the TD-B3LYP/6-311+G(2df), ROVGF/6-311+G(2df), and CCSD(T)/6-311+G(2df) levels of theory. The theoretical results are compared with the experimental data in Tables 1 and 2 for the two isomers, respectively.

The global minimum structure I has the $1a_1^2 1b_2^2 1b_1^2 2a_1^2 3a_1^2$-$2b_2^2 4a_1^2 2b_1^2 1a_2^2 3b_2^2 5a_1^2 3b_1^2$ ($^1A_1$) electronic configuration according to the ROVGF/6-311+G(2df) calculations. The calculated VDE from the $3b_1$-HOMO at three levels of theory is 2.41 eV (TD-B3LYP/6-311+G(2df)), 2.53 eV (ROVGF/6-311+G-(2df)), and 2.63 eV (CCSD(T)/6-311+G(2df)), agreeing well with the experimental value for the ground-state transition (X) with the measured VDE of 2.66 eV (Table 1). The next two detachment channels from $5a_1$-HOMO-1 and $3b_2$-HOMO-2 give very close VDEs in all three methods. Again the TD-DFT method gives slightly lower VDEs for these two detachment channels (3.14 and 3.22 eV). But the OVGF values (3.30 and 3.44 eV) are almost identical to the CCSD(T) values (3.36 and 3.44 eV), which are in excellent agreement with the experimental measurements (3.25 and 3.40 eV). The calculated VDEs from the $1a_2$-HOMO-3 and $2b_1$-HOMO-4 from TD-DFT again differ from the OVGF values, which are more reliable from

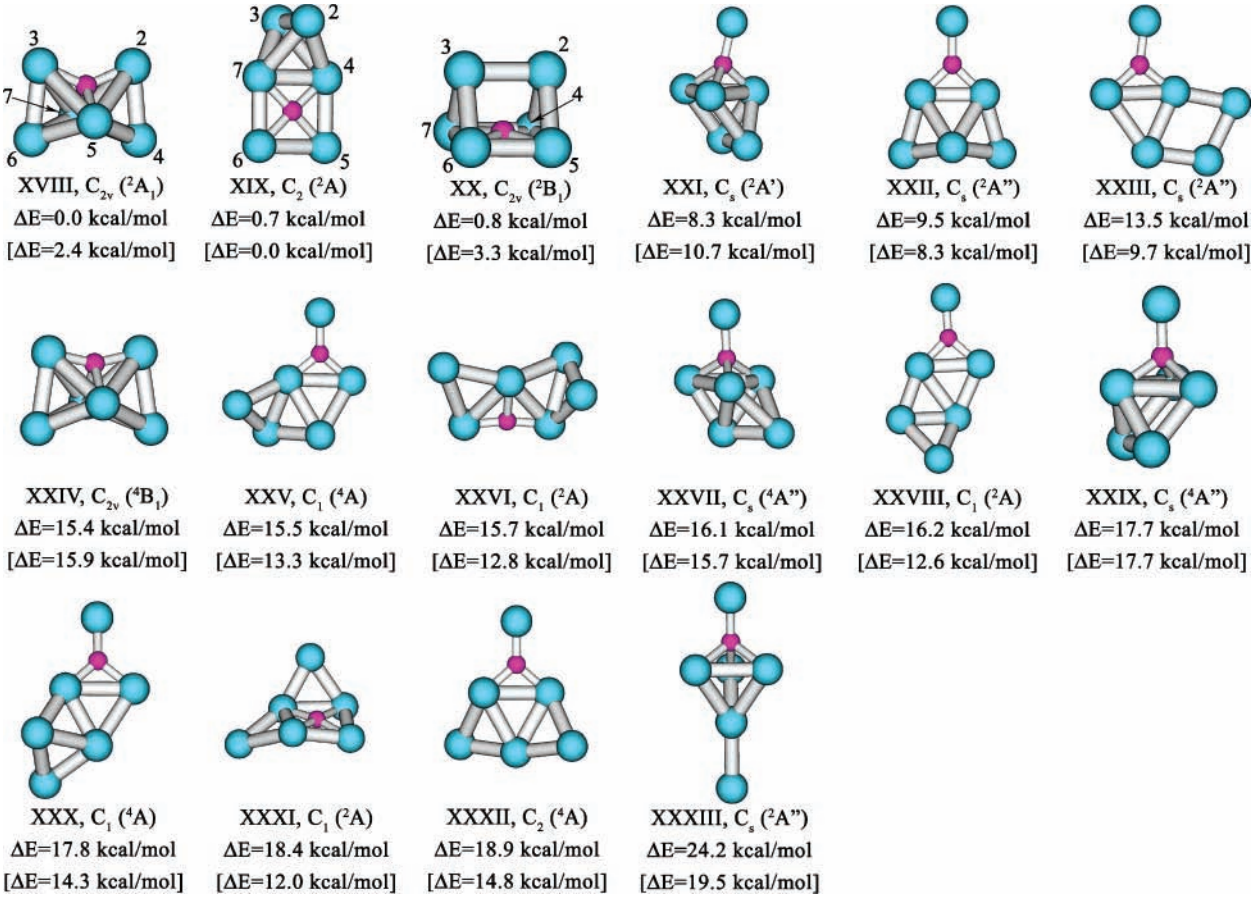

Figure 3. Computationally found isomers for Al_6N. Relative energies are given at CCSD(T)/6-311+G(2df)//B3LYP/6-311+G* and at B3LYP/6-311+G* in parentheses.

TABLE 4: Molecular Properties of the Al_6N Species Calculated at B3LYP/6-311+G*

molecular parameter	XVIII (C_{2v}, $^2A_1$)	XIX (C_2, ^2A)	XX (C_{2v}, $^2B_1$)
E, a.u.	−1509.5109768	−1509.5148164	−1509.5095013
R(N−Al_2)	1.894	3.749	2.443
R(N−Al_4)	2.832	1.886	2.003
R(N−Al_5)	2.030	1.965	
R(Al_2−Al_3)	3.499	2.579	2.712
R(Al_2−Al_4)	2.724	2.767	2.698
R(Al_2−Al_7)	3.078	2.997	
R(Al_4−Al_5)	2.700	2.730	2.934
R(Al_5−Al_6)		2.742	2.689
R(Al_4−Al_7)		2.694	
ω_1, cm^{-1}	a_1, 434 (13)	a, 714 (321)	a_1, 351 (3)
ω_2, cm^{-1}	a_1, 360 (1)	a, 408 (31)	a_1, 271 (3)
ω_3, cm^{-1}	a_1, 256 (1)	a, 301(5)	a_1, 228(0)
ω_4, cm^{-1}	a_1, 203 (1)	a, 288 (0)	a_1, 212 (35)
ω_5, cm^{-1}	a_1, 127 (0)	a, 243(4)	a_1, 193(8)
ω_6, cm^{-1}	a_1, 53 (0)	a, 172 (1)	a_2, 226 (0)
ω_7, cm^{-1}	a_2, 233 (0)	a, 70 (0)	a_2, 162 (0)
ω_8, cm^{-1}	a_2, 93 (0)	a, 63 (0)	a_2, 59 (0)
ω_9, cm^{-1}	b_1, 364 (4)	b, 639 (48)	b_1, 509 (95)
ω_{10}, cm^{-1}	b_1, 207 (12)	b, 250 (5)	b_1, 222 (4)
ω_{11}, cm^{-1}	b_1, 119 (1)	b, 221 (4)	b_1, 162 (5)
ω_{12}, cm^{-1}	b_2, 697 (108)	b, 195 (0)	b_2, 537 (160)
ω_{13}, cm^{-1}	b_2, 278 (0)	b, 123 (1)	b_2, 229 (4)
ω_{14}, cm^{-1}	b_2, 187 (0)	b, 70 (1)	b_2, 111 (5)
ω_{15}, cm^{-1}	b_2, 127 (0)	b, 34 (0)	b_2, 51 (6)

[a] Values in parentheses represent relative absorbance intensities in the IR spectrum (km/mol).

the above discussion. The OVGF values (4.20 and 4.21 eV) for these two detachment channels are somewhat larger than the experiment (4.00 and 4.06 eV). We also note that the OVGF values for the two relatively high-energy detachment channels, $4a_1$-HOMO-5 and $2b_2$-HOMO-6, are in excellent agreement with the PES data (Table 1). The pole strength (UOVGF) in the OVGF calculations was found to be between 0.81 and 0.86 for all the seven detachment channels (Table 1), indicating that electron detachments from Al_6N^- can be primarily described by one-electron processes. The overall agreement between the calculated VDEs for the structure I and the experimental VDEs is excellent.

Since the structure II was found to be very close to the global minimum structure, we also computed the VDEs for this isomer and compared them with the experimental data in Table 2. The electronic configuration for the structure II was found to be $1a_1^2$-$1b_2^2 2a_1^2 1b_1^2 3a_1^2 2b_2^2 4a_1^2 2b_1^2 3b_2^2 5a_1^2 1a_2^2 6a_1^2$ ($^1A_1$) at the ROVGF/6-311+G(2df) level of theory. The calculated VDE from the $6a_1$-HOMO at three levels of theory is 2.56 eV (TD-B3LYP/6-311+G(2df)), 2.67 eV (ROVGF/ 6-311+G(2df)), and 2.79 eV (CCSD(T)/6-311+G(2df)), which also agrees well with the experimental VDE for the ground-state transition at 2.66 eV (Table 4). However, the calculated VDEs for the higher binding energy channels completely disagree with the experiment. For example, the experiment showed that the bands A and B have very close VDEs, whereas the calculated VDEs for $1a_2$-HOMO-1 and $5a_1$-HOMO-2 show a very large separation in two methods (Table 2). The spectral pattern for the higher binding energy channels also displays a large discrepancy with the PES data. Thus, we can rule out structure II as the carrier of the PES spectra for Al_6N^-.

Our results demonstrate again the sensitivity of the calculated PES spectra to cluster structures. Even though both structures I and II are very close in total energies and give similar first

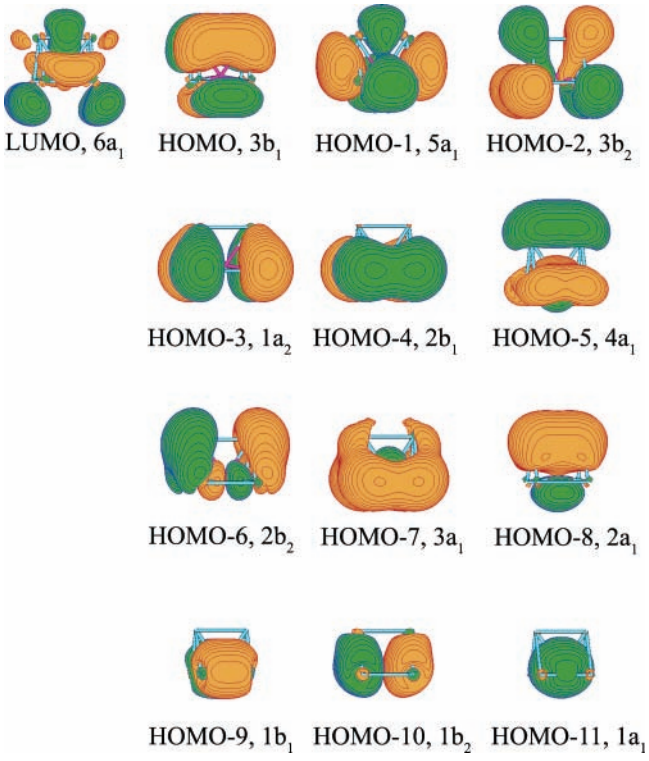

Figure 4. Molecular orbital for Al_6N^- (structure I) calculated at RHF/6-311+G*.

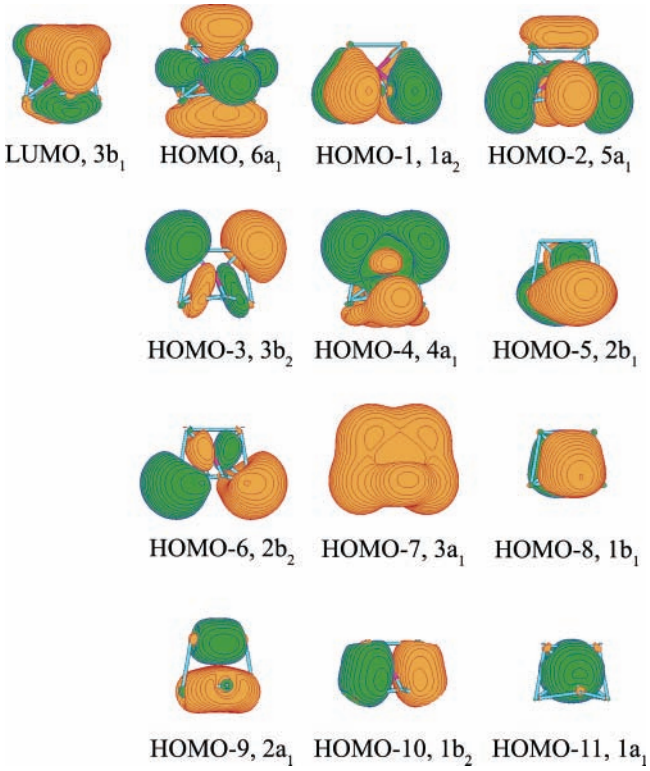

Figure 5. Molecular orbital for Al_6N^- (structure II) calculated at RHF/6-311+G*.

VDEs, their overall spectral patterns are totally different. The excellent agreement between the calculated VDEs for structure I and the experiment unequivocally confirms it as the global minimum for the Al_6N^- cluster.

7. Chemical Bonding in Al_6N^-

The global minimum structure I and the low-lying isomer II are both related to the planar tetracoordinate nitrogen molecule Al_4N^-. Our recent work[12] showed that Al_4N^- is isoelectronic to the first pentaatomic planar tetracoordinate carbon, Al_4C^{2-},[13,14] and is a very stable structural unit. We also found in that work that Al_5N^- is built upon the planar Al_4N^- unit with the extra Al bonded to one side of Al_4N^- in the same plane.[12] The ground state of Al_6N^- can be viewed as an Al_4N^- unit with the two extra Al atoms bonded to its top, whereas the low-lying isomer II can be viewed as an Al_4N^- unit with the two Al atoms bonded to each side of it on one edge. In neutral Al_6N, among the three lowest-lying isomers structures XIX and XX are built from the planar Al_4N unit. These observations suggest the robustness and stability of the planar Al_4N^- and Al_4N structural units, which may also play major roles in larger Al_xN^- clusters.

The ground-state structure I and the low-lying isomer II for Al_6N^- can also be understood as a Jahn−Teller distortion from the corresponding high-symmetry D_{3h} and O_h structures, respectively. In order to proof these structural relationships, we added an extra pair of electrons to the lowest unoccupied MO in both structures (Figures 4 and 5). Geometry optimizations for Al_6N^{3-} started from the geometries of structures I and II led to high-symmetry D_{3h} ($^1A_1'$, $1a_1'^2 1a_2''^2 1e'^4 2a_1'^2 2a_2''^2 2e'^4 1e''^4 3a_1'^2 3e'^4$) and O_h ($^1A_{1g}$, $1a_{1g}^2 1t_{1u}^6 2a_{1g}^2 2t_{1u}^6 1e_g^4 1t_{2g}^6$) structures (see MOs in Figures 6 and 7). While isolated Al_6N^{3-} is not electronically stable, it has a repulsive Coulomb barrier on the electron ejection pathway and therefore it has a certain lifetime at the optimized O_h geometry. We discuss this metastable trianion only for showing that the low-symmetry

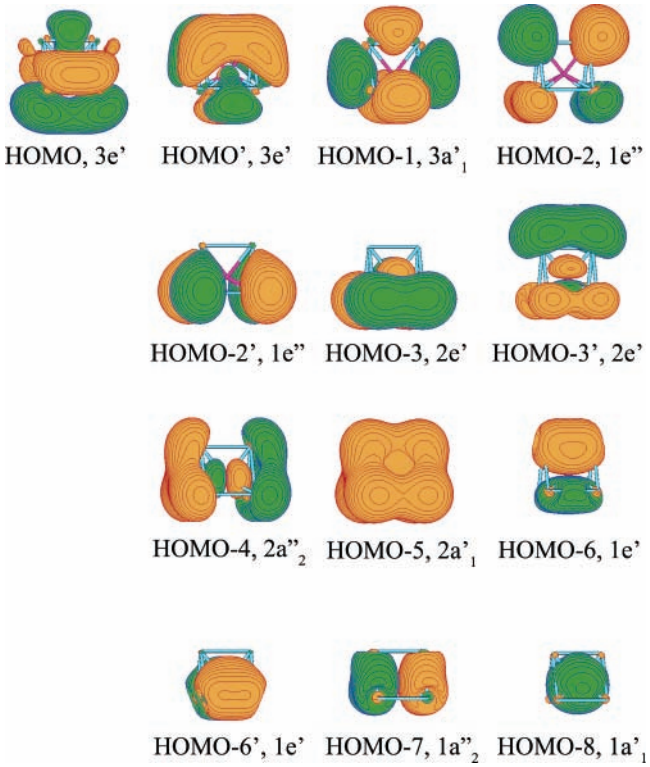

Figure 6. Molecular orbital for Al_6N^{3-} (structure D_{3h}, $^1A_1'$) calculated at RHF/6-311+G*.

global minimum structure of Al_6N^- can be explained on the basis of the Jahn−Teller effect. At the B3LYP/6-311+G* level of theory, the O_h ($^1A_{1g}$) structure is a local minimum and the D_{3h} ($^1A_1'$) structure was found to be a first-order saddle point being 8.9 kcal/mol (B3LYP/6-311+G*) and 15.2 kcal/mol (CCSD(T)/6-311+G(2df)//B3LYP/6-311+G*) higher in energy than the O_h structure. Geometry optimization of the D_{3h} ($^1A_1'$)

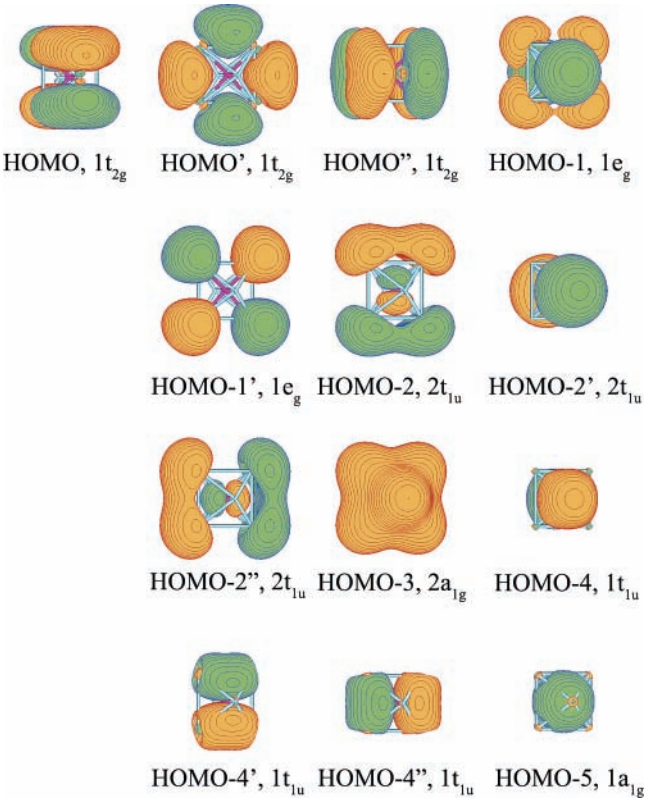

Figure 7. Molecular orbital for Al_6N^{3-} (structure O_h, $^1A_{1g}$) calculated at RHF/6-311+G*.

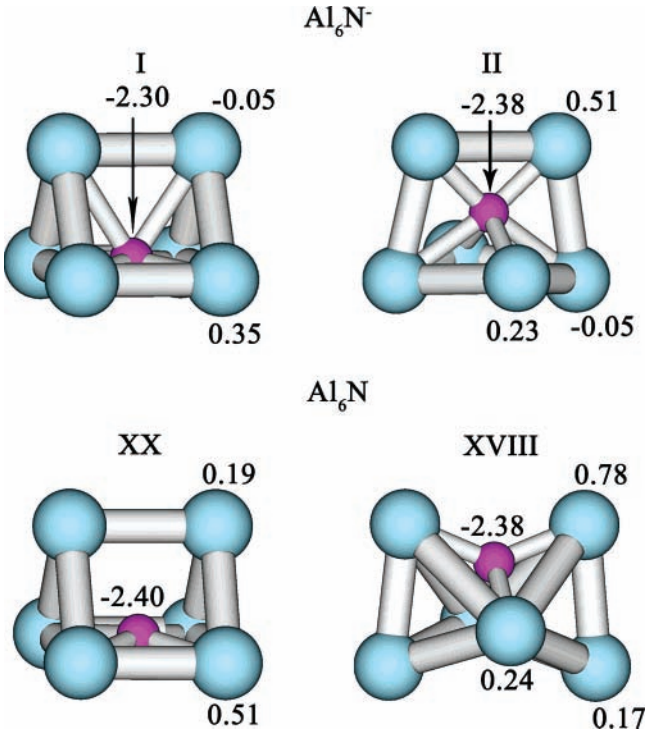

Figure 8. Effective NBO atomic charges (in |e|) for Al_6N^- (structures I and II) and Al_6N (structures XX and XVIII) at B3LYP/6-311+G*.

structure along the imaginary frequency mode led to the O_h structure. Thus, when a pair of electrons are removed from the $1t_{2g}$-HOMO (O_h) or from the 3e′-HOMO (D_{3h}), the ensuring Jahn−Teller distortion lead to the structures II and I, respectively.

Calculated NBO charges at B3LYP/6-311+G* for the two lowest structures of Al_6N^- and Al_6N are summarized in Figure 8. In all four structures the effective charge on the central N atom is almost the same (−2.30 − (−2.40) |e|), which is close to the ionic limit −3.00 |e|. Upon electron detachment from Al_6N^- the electron density is reduced primarily on aluminum atoms. That can be easily understood from the MO pictures of Al_6N^- (structures I and II) presented in Figures 5 and 6 because the $3b_1$-HOMO in the structure I and the $6a_1$-HOMO in the structure II are composed purely of aluminum AOs only. Thus, the N atom in Al_6N^- and Al_6N can be viewed as N^{3-}, consistent with the previous observation by Li and Wang that the electronic structures of Al_xN^- are similar to those of pure aluminum clusters with one less aluminum, Al_{x-1}^-.[10]

The O_h structure of Al_6N^{3-} can be related to the recently reported O_h structure of the isolated Al_6^{2-} cluster.[41] In Al_6^{2-}, the six lowest valence occupied MOs could be approximately assigned to six lone pairs formed by primarily 3s-AOs of Al with one lone pair at every Al atom. That takes 12 valence electrons out of 20. The remaining 8 valence electrons fill a completely delocalized $2a_{1g}$ MO, which is formed by the radial 3p-AOs of six aluminum atoms, and a delocalized triply degenerate $1t_{2g}$-HOMO, which is formed by the tangential 3p-AOs of the six aluminum atoms. This results in double spherical aromaticity, where the $2a_{1g}$-MO is a spherical analog of a π-aromatic MO and the $1t_{2g}$-MO is a spherical analog of σ-aromatic MOs in planar aromatic systems (see recent review ref 42 for details). MOs for the O_h structure of Al_6N^{3-} are presented in Figure 7. The lowest valence $1a_{1g}$-MO is primarily 2s-AO of the central nitrogen atom. The next triply degenerate $1t_{1u}$-MO can be assigned to three $2p_x$-, $2p_y$-, and $2p_z$-AOs of the nitrogen. The next six valence MOs ($2a_{1g}$, $2t_{1u}$, and $1e_g$) are primarily formed by the 3s-AOs of the aluminum atoms. Finally, the triply degenerate $1t_{2g}$-HOMO is formed by the tangential 3p-AOs of the Al atoms, similar to the $1t_{2g}$-HOMO in Al_6^{2-}. Thus, in the O_h structure of Al_6N^{3-} the chemical bonding can be approximately described as the central atom carrying an effective charge −3 (N^{3-}), which is ionically bound to the octahedral Al_6 cluster. The Al_6 cluster keeps its octahedral structure in Al_6N^{3-}, because N^{3-} can perfectly fit in the cavity of the octahedron and N^{3-} with its 8 valence electrons substitute a pair of electrons on the completely bonding $2a_{1g}$-MO in Al_6^{2-}. The tangential peripheral Al−Al bonding is the same in both clusters and thus Al_6N^{3-} is also tangential aromatic.

8. Conclusions

We combined photoelectron spectroscopy and theoretical calculations to elucidate the electronic structure and chemical bonding of Al_6N^-. Seven detachment channels were observed and compared with the calculated VDEs. Global minimum structures of Al_6N^- and Al_6N were identified first by using gradient embedded genetic algorithm (B3LYP/3-21G) followed by B3LYP/6-311+G* geometry and frequency calculations. The energies of the optimized structures were than refined at the CCSD(T)/6-311+G(2df)//B3LYP/6-311+G* level of theory. By comparing the theoretical VDEs with the experimental data we established that Al_6N^- has a distorted trigonal prism structure I (C_{2v}, $^1A_1$), which is built from a planar Al_4N^- unit with the two extra Al atoms bonded to its top on one side. Three low-lying isomers with close total energies were identified for the neutral Al_6N cluster, competing for the global minimum structure. The current work provides another example of the robustness and stability of the planar Al_4N unit, which may play a major structural role in larger N-doped aluminum clusters.

Acknowledgment. The theoretical work done at Utah State University was supported by The Petroleum Research Fund (ACS-PRF#43101-AC6), administered by the American Chemical Society and by the National Science Foundation (CHE-0404937). Computer time from the Center for High Performance Computing at Utah State University is gratefully acknowledged. The computational resource, the Uinta cluster supercomputer, was provided through the National Science Foundation under Grant CTS-0321170 with matching funds provided by Utah State University. The experimental work done at Washington State University was supported by the National Science Foundation (DMR-0503383) and was performed at the W. R. Wiley Environmental Molecular Sciences Laboratory, a national scientific user facility sponsored by DOE's Office of Biological and Environmental Research and located at Pacific Northwest National Laboratory, which is operated for DOE by Battelle.

References and Notes

(1) Schleyer, P. v. R.; Boldyrev, A. I. *J. Chem. Soc., Chem. Commun*. **1991**, 1536.

(2) Zakrzewski, V. G.; Niessen, W. v.; Boldyrev, A. I.; Schleyer, P. v. R. *Chem. Phys.* **1993**, *174*, 167.

(3) Nayak, S. K.; Khana, S. N.; Jena, P. *Phys. Rev. B* **1998**, *57*, 3787.

(4) Nayak, S. K.; Rao, B. K.; Jena, P.; Li, X.; Wang, L. S. *Chem. Phys. Lett*. **1999**, *301*, 379.

(5) Boo, B. H.; Liu, Z. *J. Phys. Chem. A* **1999**, *103*, 1250.

(6) Andrews, L.; Zhou, M.; Chertihin, G. V.; Bare, W. D.; Hannachi, Y. *J. Phys. A* **2000**, *104*, 1656.

(7) Leskiw, B. R.; Castleman, A. W., Jr.; Ashman, C.; Khanna, S. N. *J. Chem. Phys.* **2001**, *114*, 1165.

(8) Ling, L.; Song, B.; Cao, P.-L. *J. Mol. Struct. Theochem.* **2005**, *728*, 215.

(9) Gou, L.; Wu, H.-S. *Int. J. Quantum Chem*. **2006**, *106*, 1250.

(10) Li, X.; Wang, L. S. *Eur. Phys. J. D* **2005**, *34*, 9.

(11) Meloni, G.; Sheehan, S. M.; Parsons, B. F.; Neumark, D. M. *J. Phys. Chem. A* **2006**, *110*, 3527.

(12) Averkiev, B. B.; Boldyrev, A. I.; Li, X.; Wang, L. S. *J. Chem. Phys*. **2006**, *125*, 124305-1-12.

(13) Li, X.; Wang, L. S.; Boldyrev, A. I.; Simons, J. *J. Am. Chem. Soc.* **1999**, *121*, 6033.

(14) Li, X.; Zhang, H. F.; Wang, L. S.; Geske, G. D.; Boldyrev, A. I. *Angew. Chem., Int. Ed.* **2000**, *39*, 3630.

(15) Wang, L. S.; Cheng, H. S.; Fan, J. *J. Chem. Phys.* **1995**, *102*, 9480.

(16) Alexandrova, A. N.; Boldyrev, A. I.; Fu, Y-J.; Wang, X.-B.; Wang, L. S. *J. Chem. Phys.* **2004**, *121*, 5709.

(17) Alexandrova, A. N.; Boldyrev, A. I. *J. Chem. Theory Comput.* **2005**, *1*, 566.

(18) Becke, A. D. *J. Chem. Phys.* **1993**, *98*, 5648.

(19) Vosko, S. H.; Wilk, L.; Nusair, M. *Can. J. Phys.* **1980**, *58*, 1200.

(20) Lee, C.; Yang, W.; Parr, R. G. *Phys. Rev. B* **1988**, *37*, 785.

(21) (a) Binkley, J. S.; Pople, J. A.; Hehre, W. J. *J. Am. Chem. Soc.* **1980**, *102*, 939. (b) Gordon, M. S.; Binkley, J. S.; Pople, J. A.; Pietro, W. J.; Hehre, W. J. *J. Am. Chem. Soc.* **1982**, *104*, 2797. (c) Pietro, W. J.; Francl, M. M.; Hehre, W. J.; Defrees, D. J.; Pople, J. A.; Binkley, J. S. *J. Am. Chem. Soc.* **1982**, *104*, 5039.

(22) Cizek, J. *Adv. Chem. Phys.* **1969**, *14*, 35.

(23) Knowles, P. J.; Hampel, C.; Werner, H.-J. *J. Chem. Phys.* **1993**, *99*, 5219.

(24) Raghavachari, K.; Trucks, G. W.; Pople, J. A.; Head-Gordon, M. *Chem. Phys. Lett.* **1989**, *157*, 479.

(25) McLean, A. D.; Chandler, G. S. *J. Chem. Phys.* **1980**, *72*, 5639.

(26) Clark, T.; Chandrasekhar, J.; Spitznagel, G. W.; Schleyer, P. v. R. *J. Comput. Chem.* **1983**, *4*, 294.

(27) Frisch, M. J.; Pople, J. A.; Binkley, J. S. *J. Chem. Phys.* **1984**, *80*, 3265.

(28) Bernardi, F.; Bottini, A.; McDougall, J. J. W.; Robb, M. A.; Schlegel, H. B. *Faraday Symp. Chem. Soc*. **1979**, *19*, 137.

(29) Frisch, M. J.; Ragazos, I. N.; Robb, M. A.; Schlegel, H. B. *Chem. Phys. Lett.* **1992**, *189*, 524.

(30) Cederbaum, L. S. *J. Phys. B* **1975**, *8*, 290.

(31) Niessen, W. v.; Shirmer, J.; Cederbaum, L. S. *Comput. Phys. Rep.* **1984**, *1*, 57.

(32) Zakrzewski, V. G.; Niessen, W. v. *J. Comput. Chem.* **1993**, *14*, 13.

(33) (a) Ortiz, J. V. *Int. J. Quantum Chem., Quantum Chem. Symp*. **1989**, 23, 321. (b) Lin, J. S.; Ortiz, J. V. *Chem. Phys. Lett.* **1990**, *171*, 197.

(34) Zakrzewski, V. G.; Ortiz, J. V.; Nichols, J. A.; Heryadi, D.; Yeager, D. L.; Golab, J. T. *Int. J. Quantum Chem*. **1996**, *60*, 29.

(35) Bauernshmitt, R.; Alrichs, R. *Chem. Phys. Lett.* **1996**, *256*, 454.

(36) Casida, M. E.; Jamorski, C.; Casida, K. C.; Salahub, D. R. *J. Chem. Phys.* **1998**, *108*, 4439.

(37) Frisch, M. J.; Trucks, G. M.; Schlegel, H. B.; Scuseria, G. E.; Robb, M. A.; Cheeseman, J. R.; Zakrzewski, V. G.; Montgomery, J. A.; Stratmann, R. E.; Burant, J. C.; Dapprich, S.; Millam, J. M.; Daniels, A. D.; Kudin, K. N.; Strain, M. C.; Farkas, O.; Tomasi, J.; Barone, V.; Cossi, M.; Cammi, R.; Mennucci, B.; Pomelli, C.; Adamo, C.; Clifford, S.; Ochterski, J. W.; Petersson, G. A.; Ayala, P. Y.; Cui, Q.; Morokuma, K.; Malick, D. K.; Rabuck, A. D.; Raghavachari, K.; Foresman, J. B.; Cioslowski, J.; Ortiz, J. V.; Stefanov, B. B.; Liu, G.; Liashenko, A.; Piskorz, P.; Komaromi, I.; Gomperts, R.; Martin, R. L.; Fox, D. J.; Keith, T.; Al-Laham, M. A.; Peng, C. Y.; Nanayakkara, A.; Gonzales, C.; Challacombe, M.; Gill, P. M. W.; Johnson, B. G.; Chen, W.; Wong, M. W.; Andres, J. L.; Head-Gordon, M.; Replogle, E. S.; Pople, J. A. Gaussian 98 (revision A.1); Gaussian, Inc: Pittsburgh, PA, 1998.

(38) Frisch, M. J.; Trucks, G. W.; Schlegel, H. B.; Scuseria, G. E.; Robb, M. A.; Cheeseman, J. R.; Montgomery, J. A., Jr.; Vreven, T.; Kudin, K. N.; Burant, J. C.; Millam, J. M.; Iyengar, S. S.; Tomasi, J.; Barone, V.; Mennucci, B.; Cossi, M.; Scalmani, G.; Rega, N.; Petersson, G. A.; Nakatsuji, H.; Hada, M.; Ehara, M.; Toyota, K.; Fukuda, R.; Hasegawa, J.; Ishida, M.; Nakajima, T.; Honda, Y.; Kitao, O.; Nakai, H.; Klene, M.; Li, X.; Knox, J. E.; Hratchian, H. P.; Cross, J. B.; Bakken, V.; Adamo, C.; Jaramillo, J.; Gomperts, R.; Stratmann, R. E.; Yazyev, O.; Austin, A. J.; Cammi, R.; Pomelli, C.; Ochterski, J. W.; Ayala, P. Y.; Morokuma, K.; Voth, G. A.; Salvador, P.; Dannenberg, J. J.; Zakrzewski, V. G.; Dapprich, S.; Daniels, A. D.; Strain, M. C.; Farkas, O.; Malick, D. K.; Rabuck, A. D.; Raghavachari, K.; Foresman, J. B.; Ortiz, J. V.; Cui, Q.; Baboul, A. G.; Clifford, S.; Cioslowski, J.; Stefanov, B. B.; Liu, G.; Liashenko, A.; Piskorz, P.; Komaromi, I.; Martin, R. L.; Fox, D. J.; Keith, T.; Al-Laham, M. A.; Peng, C. Y.; Nanayakkara, A.; Challacombe, M.; Gill, P. M. W.; Johnson, B.; Chen, W.; Wong, M. W.; Gonzalez, C.; Pople, J. A. Gaussian 03, Revision C.02; Gaussian, Inc.: Wallingford, CT, 2004.

(39) Schaftenaar, G. MOLDEN3.4; CAOS/CAMM Center: The Netherlands, 1998.

(40) Wang, L. S.; Conceicao, J.; Jin, C.; Smalley, R. E. *Chem. Phys. Lett.* **1991**, *182*, 5.

(41) Kuznetsov, A. E.; Boldyrev, A. I.; Zhai, H-.J.; Li, X.; Wang, L. S. *J. Am. Chem. Soc.* **2002**, *124*, 11801.

(42) Boldyrev, A. I.; Wang, L. S. *Chem. Rev.* **2005**, *105*, 3716.